Modulation and Noise Characteristics of 1.55µm Tunneling Injection Quantum Dot Lasers

Maryam Sanaee[1], Abbas Zarifkar[2]*

Received: 2016-6-06 Accepted 2016-7-06

Abstract

In this paper, we have presented a theoretical model to investigate the modulation response, the relative intensity noise and the frequency noise characteristics of 1.55µm tunneling injection quantum dot (TI-QD) lasers. Using a small signal model based on the carriers and photon rate equations, the modulation and noise behaviour of these lasers are simulated. Our simulations imply that the modulation response of QD laser enhances in tunneling heterostructures, which is in agreement with the reported experimental results. In fact, it is demonstrated that due to tunneling of carriers directly to the ground state across a barrier, the modulation response enhances and the 3dB bandwidth of laser increases. Furthermore, the calculations indicate that the relative intensity noise level of this type of lasers increases due to decrease in the carrier population at the excited and wetting layer states. Meanwhile, the frequency noise level and linewidth show similar values to those in conventional QD lasers.

Keywords: 1.55 µm QD lasers, Tunneling injection, Relative intensity noise, Frequency noise, Modulation Response.

Introduction

Semiconductor quantum dot lasers have attracted considerable attention in high speed optical communication systems. In contrast to quantum well counterparts, QD lasers are proposed to show superior performances including low threshold current, high temperature stability, high modulation bandwidths, and low frequency chirping [1-5]. Among various systems of materials for QD lasers, InAs/InP based ones have shown great attraction in recent years since they work at the wavelength of 1.55µm, in the range which optical communication fibers show low attenuation [6-10].

Although several experimental works have reported low threshold current at room temperature [10] and low chirping [8] in some practical 1.55 µm InAs/InP QD lasers, but they have shown damped modulation response with 3dB bandwidth up to 10 GHz [10]. Recent theoretical modelling has shown that gain compression is the main reason of damping oscillation in QD lasers [11]. Meanwhile, some new approaches have been suggested such as modulating QD laser in large signal regime [11] or operating at excited state (ES) emission [12], to overcome this damping behaviour and reach higher modulation bandwidth. One of unique solutions which has been proposed and realized actually to enhance modulation bandwidth of QD lasers up to 14GHz, is utilizing tunneling injection structure [13]. In a tunnel-injection heterostructure, carriers are injected directly into the ground state (GS) of QDs through a phonon assisted tunneling process across a barrier and during a short time from an injection well [13].

Actually, in optical communication systems, modulation response and noise characteristics of laser source play an essential role. Indeed, the level of intensity and frequency noise of laser source helps to estimate the transmission data rate and possible number of channels in a single optical fibre, respectively.

Firstly, Asryan et al. showed that using tunneling injection heterostructure can provide ultrahigh temperature stability in QD lasers [14]. After that, some different groups tried to realize superior performances of such new tunneling injection QD lasers at wavelengths of 1 or 1.3µm [15, 16]. For instance, Zi et al. have demonstrated experimentally a 1.3µm InAs/GaAs tunneling injection QD laser showing 11GHz modulation bandwidth [16]. Furthermore, in an experimental research on a tunneling injection QD laser based on InAs/InP system of materials working at 1.55µm wavelength [13], a large modulation bandwidth up to 14.4 GHz was demonstrated, which is highly demanded for long-haul fibre optical communication systems. Moreover, the first measurements on the relative intensity noise (RIN) of conventional 1.55µm InAs/InP QD lasers were

2. Department of Communications and Electronics, School of Electrical and Computer Engineering, Shiraz University, Shiraz, zarifkar@shirazu.ac.ir

reported by Greedy et al. [17]. Their results showed an RIN level of -135 to-155 dB/Hz over a range of frequencies up to 10 GHz. Meanwhile, based on our knowledge, no experimental or theoretical study exist on intensity or phase noise in tunneling injection QD lasers up to now.

In the present paper, we aim to investigate the impacts of tunneling injection structure on modulation response and relative intensity and frequency noise (FN) of 1.55µm InAs/InP QD lasers from theoretical viewpoint. To reach this goal, first we have introduced the rate equations for the carrier states at injecting well and two QDs' discrete states, the photons and the phase for tunneling injection 1.55µm QD lasers. After small signal analysis of the rate equations in presence of modulation terms or Langevin noise sources, the modulation response and noise characteristics of TI-QD lasers have been evaluated, respectively. Through calculation of modulation response, 3dB bandwidth for 1.55µm InAs/InP TI-QD laser has been calculated, showing agreement with the experimental report of Bhowmick et al. [13]. In addition, the intensity noise and linewidth of TI-QD laser are obtained. Our calculations show that the RIN level of TI-QD laser increases compared to conventional QD lasers while the level of frequency noise and linewidth of them have similar values.

The outline of this paper is as follows. In section II, the theoretical modelling is presented. In section III, we will present and discuss about the calculated results of modulation and noise characteristics of TI-QD lasers in detail. Finally, in section IV, the concluding remarks are given.

Theoretical Modelling

The energy band diagram of a 1.55µm tunneling injection QD laser along with flows of its carriers and photons is depicted in Fig. 1. In this modelling, the structure of InAs/InP TI-QD laser is considered similar to that of [13]. The active region of the laser consists of n_D-folded stacks of InAs QDs tunnel heterostructures separated by 40nm $In_{0.53}Ga_{0.23}Al_{0.24}As$ barriers. In each stack, 2.5 nm $In_{052}Al_{0.48}As$ is grown as the tunneling barrier between InAs QDs and $In_{0.45}Ga_{0.55}As$ injection wells. The surface density of QDs are considered as $\rho=10\times10^{10}cm^{-2}$. The length and width of the laser cavity are also assumed to be L=700µm and W=6µm, respectively.

1. Rate of Carriers, Photons, and Phase

Each of QDs has two discrete states namely as the excited state and the ground state with four and two degeneracies, respectively. The ground state of the injection well is approximately one optical phonon higher than the ground state of QDs. In tunneling injection QD laser, the high energy electrons at the injection well enter into the first state of QDs during tunneling time of τ_{tun} directly through phonon-assisted tunneling and may tunnel back from the GS to the wetting layer (WL) at very longer time of τ_{tun}^{back}. So, in such lasers the ES of QDs is bypassed with tunneling barrier and this state has just some electron transference with the GS.

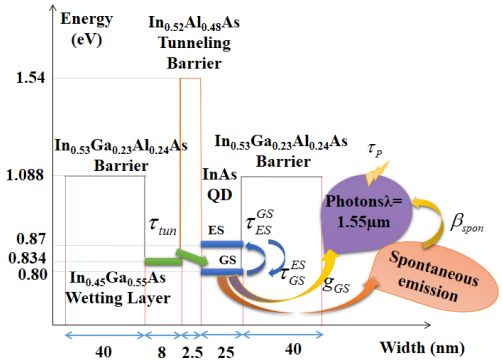

Fig. 1. The energy band diagram of 1.55µm tunneling injection QD laser besides the flows of its carriers and photons.

In fact, the flows of carriers in TI-QDL differ from the conventional QD laser in which the carriers from the wetting layer reach the lasing state after some cascading flows through the ES. According to the presented flows of carriers and photons in Fig. 1, we have written the following rate equations for the number of carriers at WL (N_{WL}), ES (N_{ES}), GS (N_{ES}), photons (S_{GS}) [18], and phase (ϕ) [19].

$$\frac{dN_{WL}}{dt}=\frac{I}{q}-\frac{N_{WL}}{\tau_{tun}}\left(1-\frac{N_{GS}}{2N_B}\right)+\frac{N_{GS}}{\tau_{tun}^{back}}-\frac{N_{WL}}{\tau_{WL}^{spon}} \quad \text{(1-a)}$$

$$\frac{dN_{ES}}{dt}=\frac{N_{GS}}{\tau_{ES}^{GS}}\left(1-\frac{N_{ES}}{4N_B}\right)-\frac{N_{ES}}{\tau_{GS}^{ES}}\left(1-\frac{N_{GS}}{2N_B}\right)-\frac{N_{ES}}{\tau_{ES}^{spon}} \quad \text{(1-b)}$$

$$\frac{dN_{GS}}{dt} = -\frac{N_{GS}}{\tau_{GS}^{spon}} + \frac{N_{WL}}{\tau_{tun}}(1-\frac{N_{GS}}{2N_B}) - \frac{N_{GS}}{\tau_{tun}^{back}} - \frac{N_{GS}}{\tau_{ES}^{GS}}(1-\frac{N_{ES}}{4N_B}) + \frac{N_{ES}}{\tau_{GS}^{ES}}(1-\frac{N_{GS}}{2N_B}) - \Gamma \upsilon_g a_{GS}(\frac{\rho}{H_e})(\frac{N_{GS}}{N_B}-1)S_{GS} \quad (1\text{-c})$$

$$\frac{dS_{GS}}{dt} = \Gamma \upsilon_g a_{GS}(\frac{\rho}{H_e})(\frac{N_{GS}}{N_B}-1)S_{GS} - \frac{S_{GS}}{\tau_P} + \beta_{sp}\frac{N_{GS}}{\tau_{GS}^{spon}} \quad (1\text{-d})$$

$$\frac{d\varphi}{dt} = (\omega_L - \omega_0) + \frac{\omega_L}{n_r}\Delta n \quad (1\text{-e})$$

where I, q, Γ, υ_g, β_{sp}, and n_r are the electrical current, the charge of an electron, the optical confinement factor, the group velocity, the spontaneous coupling factor, and the effective refractive index of gain region, respectively. The spontaneous emission times of carriers at the WL, ES, and GS are also denoted with terms $\tau_{WL(ES,GS)}^{spon}$ .The stimulated emission varies the number of carriers at the GS and is described with modal gain (g_{GS}) which is related to the differential gain of a_{GS} as follows.

$$g_{GS} = a_{GS}(\frac{\rho}{H_e})(\frac{N_{GS}}{N_B}-1) \quad (2)$$

$N_B = n\rho A$ is the total number of QDs in active media of the laser, A is the area of each QD layer, and H_e is the average height of QDs. The photon lifetime τ_p describes the escape rate of photons from the cavity and is defined below while α and $R_{1(2)}$ stand for the internal loss and the facet reflectivities, respectively.

$$\tau_p^{-1} = \upsilon_g(\alpha + \frac{1}{2L}\ln(\frac{1}{R_1R_2})) \quad (3)$$

Under quasi Fermi equilibrium, the thermal escape time of carriers from the GS to the ES has an exponential relation with its relaxation time as the following equation in which E_{ES} and E_{GS} represent the resonance energies of the ES and GS, respectively [18].

$$\tau_{ES}^{GS} = \tau_{GS}^{ES}\frac{\mu_{GS}}{\mu_{ES}}e^{(\frac{(E_{GS}-E_{ES})}{K_BT})} \quad (4)$$

In this equation, $\mu_{GS(ES)}$ represents the degeneracy of the GS (ES) and K_B and T stand for the Boltzmann constant and the temperature, respectively. Moreover, the phase rate equation shows that due to the carrier induced refractive index changes Δn, the central frequency of the laser has a finite shift called as frequency chirp. In equation (1-e), the primitive and shifted frequencies of the central longitudinal mode are denoted by ω_0 and ω_L, respectively. Similar to conventional QDL, two main mechanisms including interband transitions (IB) and free carrier absorption (FC) change the refractive index in TI-QDL which are described in the following subsections [20]. Definition and value of all parameters used in this model are listed in Table 1.

1.1. Refractive index changes due to interband transitions

The interband transitions of carriers at the WL, ES, and GS lead to the refractive index changes according to Kramers-Kronig relation as the following equations where μ_{WL} stands for the degeneracy of the WL [20].

$$\Delta n_{GS}^{IB} = -\frac{\Gamma c}{2\omega_0}\mu_{GS}a_{GS}(\frac{\rho}{H_e})(\frac{N_{GS}}{N_B}-1) = K_{GS}^{IB}(\frac{N_{GS}}{N_B}-1) \quad (5\text{-a})$$

$$\Delta n_{ES}^{IB} = -\frac{\Gamma c}{2\omega_0}\mu_{ES}a_{GS}(\frac{\rho}{H_e})(\frac{N_{ES}}{2N_B}-1) = K_{ES}^{IB}(\frac{N_{ES}}{2N_B}-1) \quad (5\text{-b})$$

$$\Delta n_{WL}^{IB} = -\frac{\Gamma c}{2\omega_0}\mu_{WL}a_{GS}(\frac{\rho}{H_e})(\frac{2N_{WL}}{\mu_{WL}N_B}-1) = K_{WL}^{IB}(\frac{2N_{WL}}{\mu_{WL}N_B}-1) \quad (5\text{-c})$$

TABLE I
NUMERICAL PARAMETERS USED IN SIMULATION

Symbol	Description	Value
v_g	Group velocity	9.17×10^{7}m.s^{-1}
n_D	Number of QD layers	10
ρ	Surface density of QDs	10×10^{14}m^{-2}
n_r	Effective refractive index of gain region	3.27
m_D^*	Effective mass of electrons in QD	0.02 m_0
m_W^*	Effective mass of electrons in WL	0.08 m_0
$\mu_{GS(ES,\,WL)}$	Degeneracy of QD levels and WL	2(4, 10)
Γ	Optical confinement factor at QDs	0.06
α	Average absorption coefficient	760m
W	Width of active region	6µm
L_a	Length of cavity	700µm
β_{spon}	Spontaneouse Emission Factor	10^{-4}
τ_{tun}	Tunneling time	5ps
τ_{GS}^{ES}	Relaxation time from ES to GS	1ps
τ_{tun}^{back}	Tunneling back time	0.55ns
a_{GS}	Differential gain	0.5×10^{-14} cm^2
$\tau_{WL(ES)}^{spon}$	Spontaneous Emission time at WL, ES	500ps
τ_{GS}^{spon}	Spontaneouse Emission time at GS	1200ps

1.2. Refractive index changes due to free carrier absorption

Furthermore, based on the plasma effect, the refractive index is changed because of free carrier absorption from the WL, ES, and GS and might be calculated by Drude model [20].

$$\Delta n_{GS}^{FC} = -\frac{\Gamma q^2}{n_r \varepsilon_0 m_D^* \omega_0^2}\left(\frac{\rho}{H_e}\right)\frac{N_{GS}}{N_B} = K_{GS}^{FC} N_{GS} \quad (6\text{-a})$$

$$\Delta n_{ES}^{FC} = -\frac{\Gamma q^2}{n_r \varepsilon_0 m_D^* \omega_0^2}\left(\frac{\rho}{H_e}\right)\frac{N_{ES}}{N_B} = K_{ES}^{FC} N_{ES} \quad (6\text{-b})$$

$$\Delta n_{WL}^{FC} = -\frac{\Gamma q^2}{n_r \varepsilon_0 m_W^* \omega_0^2}\left(\frac{\rho}{H_e}\right)\frac{N_{WL}}{N_B} = K_{WL}^{FC} N_{WL} \quad (6\text{-c})$$

Thus, the total refractive index change of Δn, is calculated by summing up the IB and FC index changes.

2. Small Signal Modulation Response

Considering a sinusoidal small signal term for injected current, the modulation response of TI-QDL can be obtained. This leads to modulations of carriers, photons, and phase defined as $\delta n_i(t)$, $\delta s_{GS}(t)$, and $\delta\varphi(t)$, respectively as below:

$$n_i(t) = N_i + \delta n_i(t)\,;\; i = WL, ES, GS \quad (7\text{-a})$$

$$s_{GS}(t) = S_{GS} + \delta s_{GS}(t) \quad (7\text{-b})$$

$$\varphi(t) = \varphi_0 + \delta\phi(t) \quad (7\text{-c})$$

Firstly, the steady state values for number of carriers (N_i), photons (S_{GS}), and central frequency (ω_0) must be calculated under pumping current of I. Then, the small signal terms of the rate equations are linearized by neglecting higher powers of the modulation terms. After taking Fourier transform of small signal rates, a closed form as a single matrix equation is obtained.

$$\sum_{l=1}^{4}[a_{ml}(\omega)]_{4\times4}.[\tilde{\delta n}_l(\omega)]_{4\times1} = [\delta\tilde{i}(\omega),0,0,0]^T_{4\times1}\;; \quad (8)$$
$$m, l = WL, ES, GS, and\ S$$

In linear small signal rate equations, the coefficients matrix is defined by $[a_{ml}]_{4\times4}$. Consequently, the modulation transfer function of TI-QDL ($IM(\omega)$) can be calculated as below.

$$IM(\omega) = \frac{\delta\tilde{s}_{GS}(\omega)}{(\delta\tilde{i}(\omega)/q)} = \frac{Det_1^4(\omega)}{H(\omega)} \quad (9)$$

In the above equation, $H(\omega)$ represents the determinant of the small signal matrix and the term Det_m^i stands for the determinant of the coefficients matrix $[a_{ml}]_{4\times4}$, in which its i-th column is replaced by a vector matrix $[V_m]_{4\times1}$. All the elements of this vector matrix are equal to zero except the m-th one, which is equal to one.

3. Correlation coefficients and Noise Characteristics

By adding the Langevin noise sources regarded to the WL, ES, GS carriers, photons and phase (F_{WL}, F_{ES}, F_{GS}, F_S, and F_ϕ, respectively) to the main and small signal rate equations, we can calculate the frequency and relative intensity noise of TI-QDL. Similar to modulation terms in equations (8), the

time dependent fluctuations should be considered for all the variables. Then as well, in noise calculations, the set of small signal rate equations are also described in a single matrix relation after applying the Fourier transform.

$$\sum_{l=1}^{4}[a_{ml}(\omega)]_{4\times4}.[\tilde{\delta}n_l(\omega)]_{4\times1}=[\tilde{F}_m(\omega)]_{4\times1}\ ; \quad (10)$$
$$m,l=WL,ES,GS,and\ S$$

Fourier transform of the Langevin noise sources and the carrier or photon fluctuations, in frequency domain ω, are represented by $\tilde{F}_m(\omega)$ and $\tilde{\delta}n_l(\omega)$, respectively. Showing no memory, the Langevin noise sources satisfy the following relations under Markovian assumptions [20].

$$\langle F_k(t)\rangle=0 \quad (11\text{-a})$$

$$\langle F_k(t)F_{k'}(t')\rangle=2D_{kk'}\delta(t-t') \quad (11\text{-b})$$

The angel brackets $\langle * \rangle$ and the term $D_{kk'}$ stand for the ensemble average and the correlation coefficients between noise sources, respectively. In fact, each of the discrete random flows of carriers or photons into or out of a state or lasing mode contributes to shot noise. Thus, the auto correlation strength of D_{kk} can be evaluated by summing over all the particles' flows into or out of the reservoir [21].

$$2D_{WW}=2(\frac{N_{WL}}{\tau_{tun}}(1-\frac{N_{GS}}{2N_B})+\frac{N_{GS}}{\tau_{tun}^{back}}+\frac{N_{WL}}{\tau_{WL}^{spon}}) \quad (12\text{-a})$$

$$2D_{EE}=2(\frac{N_{ES}}{\tau_{GS}^{ES}}(1-\frac{N_{GS}}{2N_B})+\frac{N_{GS}}{\tau_{ES}^{GS}}(1-\frac{N_{ES}}{4N_B})+\frac{N_{ES}}{\tau_{ES}^{spon}}) \quad (12\text{-b})$$

$$2D_{GG}=2(\Gamma\upsilon_g a_{GS}(\frac{\rho}{H_e})(\frac{N_{GS}}{N_B}-1)S_{GS}+\frac{N_{WL}}{\tau_{tun}}(1-\frac{N_{GS}}{2N_B})+\frac{N_{GS}}{\tau_{tun}^{back}}+\frac{N_{ES}}{\tau_{GS}^{ES}}(1-\frac{N_{GS}}{2N_B})+\frac{N_{GS}}{\tau_{ES}^{GS}}(1-\frac{N_{ES}}{4N_B})+\frac{N_{GS}}{\tau_{GS}^{spon}}) \quad (12\text{-c})$$

$$2D_{SS}=2(\Gamma\upsilon_g a_{GS}(\frac{\rho}{H_e})(\frac{N_{GS}}{N_B}-1)S_{GS}+\frac{S_{GS}}{\tau_P}+\beta_{sp}\frac{N_{GS}}{\tau_{GS}^{spon}}) \quad (12\text{-d})$$

In fact, when a state or a lasing mode gains a particle ($F_k>0$), the other reservoir loses a particle ($F_{k'}<0$) and hence, the correlation between each pair of different noise sources is negative. So, we can calculate the cross correlation coefficients $D_{kk'}$ by tallying the flows of carriers or photons which affect both reservoirs simultaneously [21].

$$D_{WG}=-(\frac{N_{WL}}{\tau_{tun}}(1-\frac{N_{GS}}{2N_B})+\frac{N_{GS}}{\tau_{tun}^{back}}) \quad (13\text{-a})$$

$$D_{EG}=-(\frac{N_{ES}}{\tau_{GS}^{ES}}(1-\frac{N_{GS}}{2N_B})+\frac{N_{GS}}{\tau_{ES}^{GS}}(1-\frac{N_{ES}}{4N_B})) \quad (13\text{-b})$$

$$D_{GS}=-\Gamma\upsilon_g a_{GS}(\frac{\rho}{H_e})(\frac{N_{GS}}{N_B}-1)S_{GS} \quad (13\text{-c})$$

Moreover, the cross correlation coefficients of D_{WS}, D_{ES}, and D_{WE} are equal to zero, since just the GS carriers have transference with the WL, ES, and photons reservoirs.

3.1. Relative Intensity Noise

Actually, upon the discrete and random nature of the carrier generation and recombination processes, the output power of QD laser shows some random fluctuations around its operation point. The intensity noise of TI-QDL which is manifestation of the mentioned fluctuations is characterized by the relative intensity noise (RIN) per unit bandwidth as below [21]:

$$\frac{RIN}{\Delta f}=\frac{S_p(\omega)}{S_{GS}{}^2} \quad (14)$$

The spectral density of $S_p(\omega)=\int_{-\infty}^{+\infty}\langle\delta s_{GS}(t+\tau)\delta s_{GS}(t)\rangle\exp(-i\omega t)d\tau$ is related to $\tilde{\delta}s_{GS}(\omega)$, by replacing the ensemble average with a time average over interval T [21].

$$S_p(\omega)=\lim_{T\to\infty}\frac{1}{T}\int_{-\frac{T}{2}}^{\frac{T}{2}}\tilde{\delta}s_{GS}(\omega)\tilde{\delta}s_{GS}{}^*(\omega)d\tau=|\tilde{\delta}s_{GS}(\omega)|^2 \quad (15)$$

Therefore, by solving the matrix equation (10), the total spectrum of photon fluctuations is calculated as [22].

$$\tilde{\delta}s_{GS}(\omega)=\frac{\sum_{m=1}^{4}Det_m^4(\omega)\tilde{F}_m(\omega)}{H(\omega)} \quad (16)$$

Consequently, $RIN(\omega)$ can be evaluated from the defined functions where Re( ) stands for the real part [22].

$$\frac{RIN(\omega)}{\Delta f}=\frac{1}{S_{GS}{}^2\left|H(\omega)\right|^2}\left(\sum_{m=1}^{4}2D_{m,m}\left|Det_m^4\right|^2+\sum_{l=1}^{4}\sum_{m=1}^{4}2D_{m,l}\,\mathrm{Re}(Det_m^4.Det_m^{4*})\right) \quad (17)$$

3.2. Frequency Noise

On the other hand, the electric field of optical beam shows both the in-phase and out-phase random fluctuations as illustrated in complex plane in Fig.2.

The total instantaneous field $E(t)$ and its associated complex Langevin noise source $F_E(t)$ are related as follow, where the in-phase and out-phase random fields are denoted by $\delta E_r(t)$ and $\delta E_i(t)$, respectively [23].

$$E(t)=E_0+\delta E_r(t)+i\,\delta E_i(t) \quad (18\text{-a})$$

$$F_E(t)=F_r(t)+iF_i(t) \quad (18\text{-b})$$

Here, the in-phase and out-phase noise sources of the optical field are represented by $F_r(t)$ and $F_i(t)$, respectively.

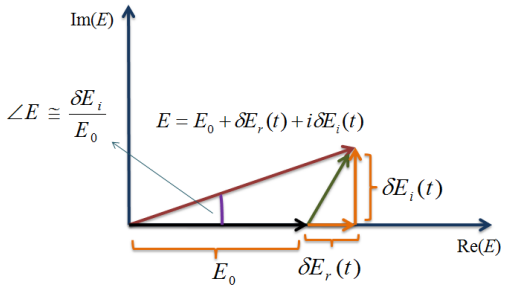

Fig. 2. Vector illustration of the relationship between the instantaneous field magnitude and the in-phase and out-phase noise components [23].

As illustrated in Fig. 2, the Langevin noise sources of the photon ($F_S(t)$) and phase ($F_\phi(t)$) can be related to the in-phase and out-phase fluctuations as follows [23].

$$\left\langle F_rF_r\right\rangle=\frac{1}{4S_{GS}}\left\langle F_SF_S\right\rangle \quad (19\text{-a})$$

$$\left\langle F_\phi F_\phi\right\rangle=\frac{1}{S_{GS}}\left\langle F_iF_i\right\rangle=\frac{1}{4S_{GS}{}^2}\left\langle F_SF_S\right\rangle \quad (19\text{-b})$$

On account of this fact that the phase fluctuation is the secondary effect of the carriers and photon noises, the phase Langevin source is inherently uncorrelated to the carrier and photon noise sources. Therefore, the cross correlation coefficients $\langle F_\varphi F_S\rangle$ and $\langle F_\varphi F_{WL(ES,GS)}\rangle$ are equal to zero. As long as the phase variations lead to frequency fluctuations through the relation $2\pi\delta\upsilon_L=\delta\dot{\varphi}(t)$, we can calculate the spectral density of the frequency noise by taking ensemble average of $\delta\dot{\varphi}(t)$ [23].

$$FN(\omega)=\frac{1}{4\pi^2}\int_{-\infty}^{+\infty}\left\langle\delta\dot{\phi}(t+\tau)\delta\dot{\phi}(t)\right\rangle e^{(-i\,\omega\tau)}d\tau \quad (20)$$

Under Markovian assumptions, simply we can obtain the spectral density of the frequency noise as follows [23].

$$FN(\omega)=\frac{1}{4\pi^2}\left\langle\left|\omega\delta\tilde{\phi}(\omega)\right|^2\right\rangle \quad (21)$$

The Fourier transform of the phase fluctuation is represented by $\delta\tilde{\varphi}(\omega)$ which is calculated by the small signal rate equation for the phase in frequency domain.

$$i\,\omega\delta\tilde{\phi}(\omega)=\frac{\omega_L}{n_r}\delta(\Delta\tilde{n}(\omega))+\tilde{F}_\phi(\omega) \quad (22)$$

Fourier transform of the small signal fluctuations of the refractive index changes $\delta(\Delta\tilde{n}(\omega))$ can be evaluated as a function of the carrier fluctuations.

$$\delta(\Delta\tilde{n}(\omega))=\sum_{i=WL,ES,GS}(K_i^{IB}+K_i^{FC})\delta\tilde{n}_i(\omega) \quad (23)$$

Each of the carrier fluctuations $\delta\tilde{n}_i(\omega)$ can be calculated versus four Langevin noise sources of the carriers and photons using equation (10). After some manipulation, frequency noise is obtained as below.

$$FN(\omega)=\frac{1}{4\pi^2}(FN_{GS}+FN_{ES}+FN_{WL}+2FN_{WL,ES}+2FN_{WL,GS}+2F_{ES,GS})+\frac{1}{16\pi^2S_{GS}{}^2}D_{SS} \quad (24)$$

The terms FN_m and $FN_{m,l}$ (m, l=WL, ES, GS) denote the self-frequency noises from each of the carrier states and the mutual frequency noises from each pair of them, respectively.

In the following section, based on above theoretical modelling, we will present the calculated results and discuss about the modulation response, the frequency and relative intensity noise

characteristics of 1.55μm tunneling injection QD lasers.

Results and Discussion

To study the modulation response and noise characteristics of 1.55μm tunneling injection QD lasers, first we have calculated the steady state number of carriers and photons under constant injection currents. The Light-Current characteristics of both tunneling injection and conventional QD lasers are plotted simultaneously in Fig. 3. To have a realistic comparison between tunneling and conventional QD lasers, we have considered the model of typical 1.55μm QD lasers [18], with the same structural parameters. It is revealed that the output power of TI-QDL is slightly higher than conventional QD laser. From physical viewpoint, by injecting electrons directly into the lasing state of QDs (GS) in a shorter tunneling time rather than in conventional QDLs, the rate of carrier injection to the GS increases which leads to higher stimulated emission rate in tunneling injection QDLs.

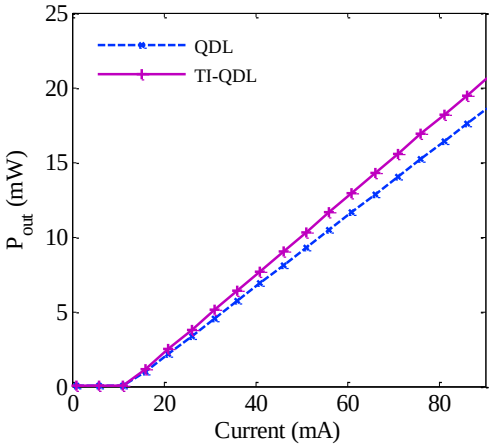

Fig. 3. The Light-Current characteristics of tunneling injection (TI) and conventional QD lasers.

Based on the above theoretical model, the calculated modulation response of both tunneling injection and conventional QD lasers at two different bias currents is shown in Fig. 4. It is demonstrated that at higher bias currents, the modulation responses of both QD laser structures broaden and their 3dB bandwidth increases. But, the modulation bandwidth in tunneling injection QD laser is higher. In fact, bypassing the injecting carriers in the WL from capturing to the ES causes that the carriers reach to the GS directly at a higher rate and hence the stimulated emission can follow modulated current faster. Therefore, the modulation bandwidth increases in TI-QD lasers. Moreover, as can be seen in Fig. 4, in conventional QD lasers, the highest modulation bandwidth is limited to 10GHz which is in agreement with the experimental reports [10]. Meanwhile, the experimental results on 1.55μm tunneling injection QD lasers show that their bandwidth may increase up to 14GHz at bias current of I=60mA [13]. Our results on modulation response of TI-QDLs are validated by the mentioned report on such lasers [13]. The 3dB bandwidth of TI-QD laser is plotted versus current in Fig. 5. It is depicted that by pumping TI-QD laser at higher currents, we can modulate the laser electrically at higher frequencies. Physically, the number of photons plays an essential role on value of the relaxation oscillation frequency in lasers. In fact, at higher currents, the rate of energy transference between carriers and photons grows which leads to a higher resonant frequency (RF) in QD lasers.

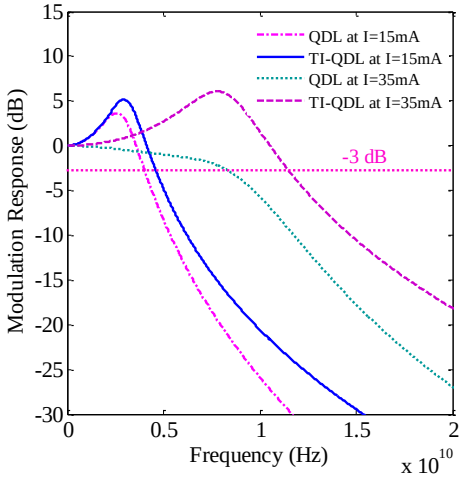

Fig. 4. Modulation responses of tunneling injection and conventional QD lasers at two currents of 15 and 35mA.

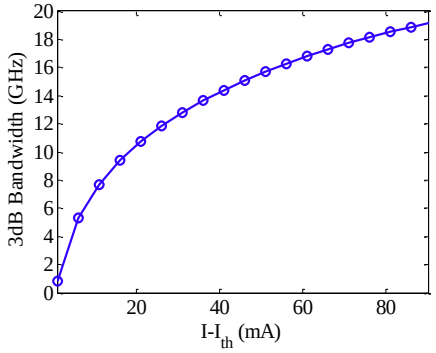

Fig. 5. The 3dB bandwidth of TI-QD laser versus injection current.

We have plotted the turn-on dynamics of carriers and photons for a current step of I=55mA, for both conventional and tunneling injection QD lasers in Fig. 6(a) to (d). It is depicted that in tunneling injection QD laser, the carrier numbers at all three states of WL, ES, and GS grow during shorter delay times. It is also shown that in TI-QDL, the population of carriers in the WL and ES is lower compared to those in conventional QD laser. Actually, by injecting carriers to the GS during a very short time interval and through a tunneling barrier, the number of carriers at the WL and ES decrease. Furthermore, in tunneling injection laser, the number of photons also reaches to its steady state point with a higher speed which is in agreement with the above results for modulation response.

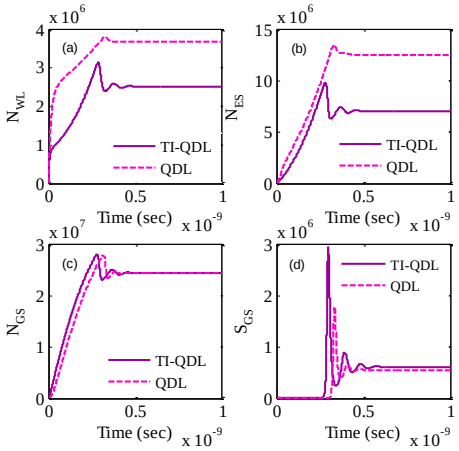

Fig. 6 (a) to (d). Turn-on dynamics of carriers and photons for a current step of I=55mA, for conventional and tunneling injection QD lasers.

The RIN spectrum of tunneling injection and conventional QD lasers at current of I=35mA, are plotted in Fig. 7. It is revealed that the spectrum of RIN in both cases has a level between -144 and -152dB/Hz at different frequencies till the resonance frequency. Furthermore, the level of RIN in tunneling injection QD laser is slightly higher than that in conventional ones. Physically, the tunneling flows of carriers from the WL to the GS occur during very shorter time interval which makes this process to have more inherent randomness. Therefore, the auto correlation coefficients associated to the WL and GS increase in tunneling structures which leads to higher intensity noise level in TI-QDLs.

Moreover, to investigate the contribution of each reservoir in total value of RIN in tunneling injection QD lasers, we have divided the auto and cross correlation terms resulted from different carrier and photon reservoirs into three groups, called WL, Quantum, and Photon noises separately. Fig. 8(a) to (c), show the values of the mentioned noise sources versus current at frequency of f=1GHz for both TI and conventional QD lasers. It is depicted that the level of all intensity fluctuations decrease by increasing the bias current and among them, the Photon and Quantum noise sources play the dominant role in overall value of RIN in both QD laser structures.

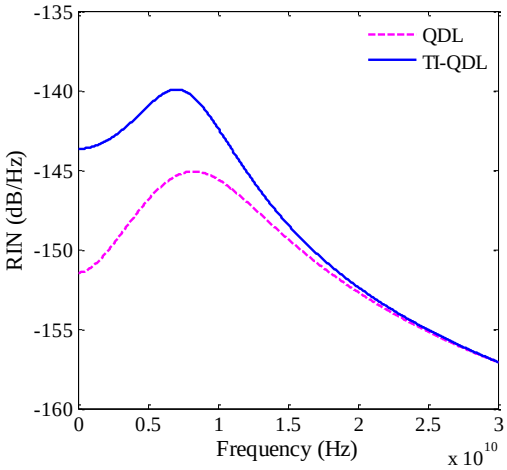

Fig. 7. Relative intensity noise (RIN) spectrum of both tunneling injection and conventional QD lasers at the injection current of I=35mA.

In fact, these results reveal that the rates of carrier transference between QD states and photon generations are higher than the rate of carrier flows to the WL. Furthermore, the levels of WL and Quantum noise sources in tunneling injection QD laser are higher compared to those in conventional QDL. Physically, it is evident that tunneling injection process makes the carrier populations at the WL and ES lower than those in conventional QD laser. So, this reduction in the WL and ES populations increases their relative fluctuations around the bias point which consequently increases the level of intensity noise in TI-QDLs.

To investigate the frequency fluctuations of TI-QD laser under small signal modulation, the spectral density of frequency noise due to each of individual carrier states and photon shot noise and the total FN spectrum are shown in Fig. 9(a) and

(b), respectively, for an injection current of I=35mA. It is deduced that among the states, the value of the noise sources from the GS and then ES are more dominant, respectively. It should also be noted that the peak of the FN spectrum at the resonant frequency of f=7.5GHz is observable in Fig. 9. In addition, according to Eq. (12-d), the auto correlation coefficient of photons is frequency independent and the FN due to photons has a comparatively low constant value at all frequencies.

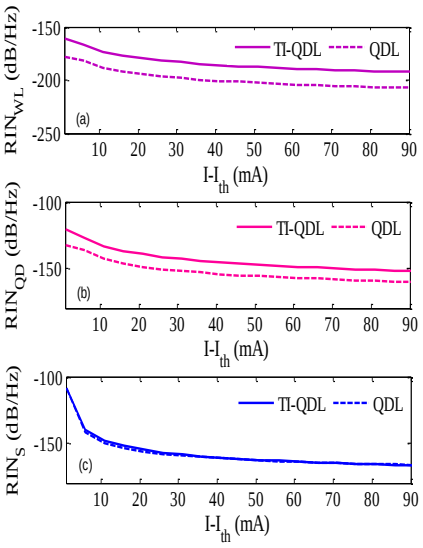

Fig. 8. (a) to (c).The values of WL, Quantum and Photons noise sources, respectively versus current at f=1GHz, for both TI and conventional QD lasers.

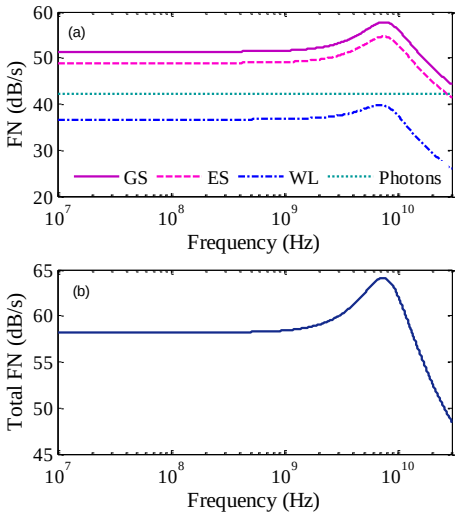

Fig. 9. (a) Spectral density of frequency noise from each individual carrier states and photon shot noise, (b) the total FN spectrum for TI-QD lasers at I=35mA.

From frequency noise calculations, the linewidth of QD laser can be evaluated under small signal modulation [19]. In Fig. 10, the linewidth of both tunneling injection and conventional QD lasers are depicted as a function of bias current. It is revealed that the linewidth of these two laser structures are similar and decreases with increasing the output power. In fact, using tunneling structure decreases the number of carriers at the WL and ES which leads to higher relative carrier fluctuations from these states. But, on the other hand, tunneling injection increases the number of photons which results in lower photon shot noises. Consequently, these two inverse impacts of carriers and photons fluctuations make the overall value of frequency noise and hence the linewidth of TI-QD lasers unchanged compared to conventional QD lasers.

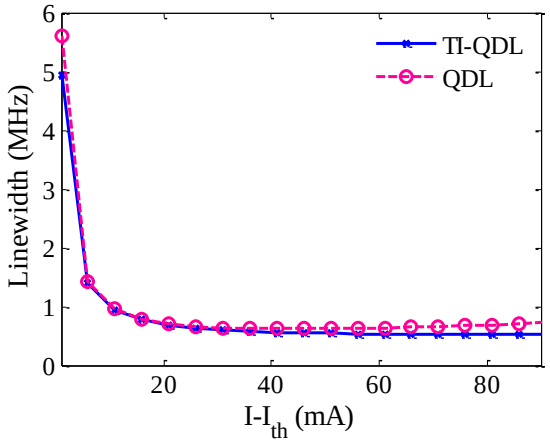

Fig. 10. Calculated linewidth of both tunneling injection and conventional QD lasers versus current.

Conclusion

The modulation response, relative intensity noise, and frequency noise characteristics of 1.55μm tunneling injection QD lasers have been studied theoretically. Through analysis of the rate equations for carriers and photons in small signal regime, it is revealed that the modulation response of QD laser improves in tunnelling heterostructure. Actually, it is shown that by tunneling injection of carriers directly to the GS through a barrier, the 3dB bandwidth of the laser increases which is in good agreement with reported experimental results. Furthermore, tunneling process helps the laser to turn-on during a shorter delay time. On the other hand, calculations show that the RIN level of TI-QD laser increases due to reduction of carrier populations at the ES and WL. It is also

demonstrated that the level of frequency noise and linewidth are similar in both tunneling injection and conventional QD lasers. In summary, it is shown that in presence of tunneling injection process, the dynamic response of QD laser enhances significantly while its intensity noise increases and its frequency noise level remains unchanged in comparison with conventional QD laser.

References

[1] T. J. Badcock, R. J. Royce, D. J. Mowbray, M. S. Skolnick, H. Y. Liu,

[2] M. Hopkinson, K. M. Groom, and Q. Jiang, "Low Threshold Current Density and Negative Characteristic Temperature 1.3μm InAs Self-Assembled Quantum Dot Lasers,"*Appl. Phys. Lett.*, vol. 90, no. 111102, pp. 1-3, 2007.

[3] K. C. Kim, K. Han, Y. C. Yoo, J. Lee, Y. M. Sung, and T. G. Kim, "Optical Characteristics and the Linewidth Enhancement Factor Measured from InAs/GaAs Quantum Dot Laser Diodes,"*IEEE Trans. Nanotech.*, vol. 7, no. 2, pp. 135-139, 2008.

[4] P. F. Xu, T. Yang, H. M. Ji, Y. L. Cao, Y. X. Gu, Y. Liu, W. Q. Ma, and Z. G. Wang, "Temperature-Dependent Modulation Characteristics for 1.3μm InAs/GaAs Quantum Dot Lasers," *Jpn. J. Appl. Phys.*, vol. 107, no. 013102, pp. 1–5, 2010.

[5] L. Drzewietzki, G. A.P. Thè, M. Gioannini, S. Breuer, W. Elsäßer, M. Hopkinson, M. Krakowski, and I. Montrosset, "Theoretical and Experimental Investigations of the Temperature Dependent Continuous Wave Lasing Characteristics and the Switch-on Dynamics of an InAs/InGaAs Quantum-Dot Semiconductor Laser," *Optics Comm.*, vol. 283, pp. 5092-5098, 2010.

[6] C. Liu, H. Wang, and Q. Meng, "Characterization and Analysis of 1.3-μm InAs/InGaAs Self-Assembled Quantum Dot Lasers,"*IEEE Trans. Nanotech.*, vol. 13, no. 3, pp. 446-451, 2014.

[7] D. Zhou, R. Piron, F. Grillot, O. Dehaese, E. Homeyer, M. Dontabactouny, T. Batte, K. Tavernier, J. Even, and S. Loualiche, "Study of the Characteristics of 1.55μm Quantum Dash/Dot Semiconductor Lasers on InP Substrate,"*App. Phys. Lett.*, vol. 93, no. 161104, pp. 1–3, 2008.

[8] P. M. Smowton, S. N. Elliott, S. Shutts, M. S. Al-Ghamdi, and A. B. Krysa, "Temperature-Dependent Threshold Current in InP Quantum-Dot Lasers," *IEEE Selec. Topics Quantum Electron*., vol. 17, no. 5,pp. 1343-1348, 2011.

[9] Z. J. Jiao, Z.G. Lu, J.R. Liu, P.J. Poole, P.J. Barrios, D. Poitras, J. Caballero, X.P. Zhang, and G. Pakulski, "Linewidth Enhancement Factor of InAs/InP Quantum Dot Lasers around 1.5 μm," *Optics Comm.*, vol. 285, pp. 4372-4375, 2012.

[10] S.G. Li, Q. Gong, C. F. Cao, X. Z. Wang, P. Chen, L. Yue, Q. B. Liu, H. L. Wang, C. H. Ma, "Temperature Dependent Lasing Characteristics of InAs/InP(100) Quantum Dot Laser," *Mat. Sci. Semic. Procc*., vol. 15, pp. 86-90, 2012.

[11] D. Gready, G. Eisenstein, V. Ivanov, C. Gilfert, F. Schnabel, A. Rippien, J. P. Reithmaier, and C. Bornholdt, "High Speed 1.55 μm InAs/InGaAlAs/InP Quantum Dot Lasers," *IEEE Phot. Tech. Lett*., vol. 26, no. 1, pp. 11-13, 2014.

[12] D. Gready, G. Eisenstein, M. Gioannini, I. Montrosset, D. Arsenijevic, H. Schmeckebier, M. Stubenrauch, and D. Bimberg, "On the Relationship between Small and Large Signal Modulation Capabilities in Highly Nonlinear Quantum Dot Lasers,"*App. Phys. Lett.*, vol. 102, no. 101107, pp. 1-3, 2013.

[13] C. Wang, B. Lingnau, K. Ldge, J. Even, and F. Grillot, "Enhanced Dynamic Performance of Quantum Dot Semiconductor Lasers Operating on the Excited State," *IEEE J. Quantum Electron*. vol. 50, no. 9, pp. 723-731, 2014.

[14] S. Bhowmick, M. Z. Baten, T. Frost, B. S. Ooi, and P. Bhattacharya, "High Performance InAs/$In_{0.53}Ga_{0.23}Al_{0.24}As$/InP Quantum Dot 1.55 μm Tunnel Injection Laser," *IEEE J. Quantum Electron*., vol. 50, no. 11, pp. 7-14, 2014.

[15] L. V. Asryan and S. Luryi, "Tunneling-Injection Quantum-Dot Laser: Ultrahigh Temperature Stability," *IEEE J. Quantum Electron*., vol. 37, no. 7, pp. 905-910, 2001.

[16] P. Bhattacharya, S. Ghosh, S. Pradhan, J. Singh, Z. K. Wu, J. Urayama, K. Kim, and T. B. Norris, "Carrier Dynamics and High-Speed Modulation Properties of Tunnel Injection InGaAs–GaAs Quantum-Dot Lasers," *IEEE J. Quantum Electron*., vol. 39, no. 8, pp. 952-962, 2003.

[17] Z. Mi, P. Bhattacharya, and S. Fathpour, "High-speed 1.3*μm* tunnel injection quantum-dot lasers," *App. Phys. Lett.*, vol. 86, no. 153109, pp. 1-3, 2005.

[18] D. Gready, G. Eisenstein, C. Gilfert, V. Ivanov, and J. P. Reithmaier, "High-Speed Low-Noise InAs/InAlGaAs/InP 1.55-μm Quantum-Dot Lasers," *IEEE Phot. Tech. Lett*., vol. 24, no. 10, pp. 809-811, 2012.

[19] C. Wang, F. Grillot, and J. Even, "Impacts of Wetting Layer and Excited State on the Modulation Response of Quantum-Dot Lasers," *IEEE J. Quantum Electron*., vol. 48, no. 9, pp. 1144-1150, 2012.

[20] G. P. Agrawal and N. K. Dutta, *Semiconductor Lasers*. Van Nostrand Reinhold, pp. 232-275, 1993.

[21] J. Kim, C. Meuer, D. Bimberg, and G. Eisentein, "Numerical Simulation of Temporal and Spectral Variation of Gain and Phase Recovery in Quantum-Dot Semiconductor Optical Amplfiers," *IEEE J. Quantum Electron*., vol. 46, no. 3, pp. 405-413, 2010.

[22] M. Sanaee, and A. Zarifkar, "Theoretical Modeling of Relative Intensity Noise in p-doped 1.3μm InAs/GaAs Quantum Dot Lasers,"*IEEE J. Lightwave Tech*., vol. 33, no. 1, pp. 234-243, 2015.

[23] M. Sanaee, and A. Zarifkar, "Effect of Carrier Transition Mechanisms and Gain Compression on Relative Intensity Noise of 1.55μm QD Lasers," *Optics Comm.*, vol. 353, pp. 42-48, 2015.

[24] L. A. Coldren, S. Corzine and M. Mashanovitch, *Diode Lasers and Photonic Integrated Circuits*, J. Wiely& Sons, pp. 661-672, 2012.